

# Structure and electrical properties of p-type twin ZnTe nanowires

Shanying Li · Yang Jiang · Di Wu · Binbin Wang ·  
Yugang Zhang · Junwei Li · Xinmei Liu ·  
Honghai Zhong · Lei Chen · Jiansheng Jie

Received: 23 September 2010 / Accepted: 15 December 2010 / Published online: 6 January 2011  
© Springer-Verlag 2011

**Abstract** Resonant tunneling is firstly found in twin p-type ZnTe nanowire field-effect transistors. The twin ZnTe nanowires are synthesized via the thermal evaporation process. X-ray diffraction and high-resolution transmission electron microscopy characterization indicate that the as-grown twin nanowire has a zinc-blende crystal structure with an integrated growth direction of [11-1]. The twin plane is (11-1) and the angle between the mirror symmetrical planes is  $141^\circ$ . The formation of twins is attributed to the surface tension from the eutectic liquid droplet. Field-effect transistors based on single ZnTe twin nanowire are constructed, the corresponding electrical measurements demonstrate that the twin nanowires have a p-type conductivity with a mobility ( $\mu_h$ ) of  $0.11 \text{ cm}^2 \text{ V}^{-1} \text{ S}^{-1}$ , and a carrier concentration ( $n_h$ ) of  $1.1 \times 10^{17} \text{ cm}^{-3}$ . Significantly, the negative differential resistance with a peak-to-valley current ratio of about 1.3 is observed in p-type twin ZnTe nanowire field-effect transistors at room temperature. As the periodic barriers produced in the periodic twin interfaces can form

multi-barrier and multi-well along one-dimensional direction. The multibarrier can be modulated under external electrical field. When the resonant condition is met, the space charge will be enhanced with the inherent feedback mechanism, and the resonant tunneling will occur.

## 1 Introduction

One-dimensional (1D) nanostructures have been considered as ideal building blocks for nanoelectronics, nano-optoelectronics, nanosensors, nanobiotechnology, and energy harvesting applications [1–9], whose properties can be influenced by their structures, morphologies, and sizes. As one member of 1D nanostructure, nanowires (NWs) or nanoribbons (NRs) with twin structures have attracted great research interests due to novel geometric shape and crystal symmetry [10, 11]. Usually, during the growth process, a twin structure can occur spontaneously because of the lower formation energy, even under well-controlled crystallization conditions. Until now, several nanostructure twins have been reported. The ZnS bicrystalline NRs were synthesized using chemical vapor deposition by Liu et al., which were used to fabricate UV sensors and optoelectronic nanodevices [12]. The formation and photoelectric properties of the periodic twin ZnSe/SiO<sub>2</sub> nanocables were also presented by Fan et al. [13]. Davidson et al. have studied the lamellar twinning in semiconductor NWs. and presented a semiquantitative model to explain the twin formation mechanism in III–V and IV groups NWs [14]. The formation of twinning modulation ZnSe NWs with a defect-related photoluminescence emission has been reported by Wang et al. [15]. The twin existed in 1D ZnO nanostructures have also been presented by Ding et al. [16].

---

S. Li · Y. Jiang (✉) · D. Wu · B. Wang · Y. Zhang · J. Li · X. Liu ·  
H. Zhong · L. Chen  
School of Materials Science and Engineering, Hefei University of  
Technology, Hefei, Anhui 230009, People's Republic of China  
e-mail: [apjiang@hfut.edu.cn](mailto:apjiang@hfut.edu.cn)

S. Li  
Department of Chemical Engineering, Henan University of Urban  
Construction, Pingdingshan, Henan 467036, People's Republic of  
China

Y. Zhang · J. Jie  
School of Electronic Science and Applied Physics,  
Hefei University of Technology, Hefei, Anhui 230009,  
People's Republic of China

J. Jie  
e-mail: [jsjie@hfut.edu.cn](mailto:jsjie@hfut.edu.cn)

As an important direct band semiconductor material of II–VI group, ZnTe has a direct band-gap of 2.26 eV at room temperature. The applications of ZnTe in green light emitting diodes, X-ray detectors and solar cells have been well recognized [2, 17–20]. Interestingly, the intrinsic ZnTe usually exhibits p-type conductivity and this character can be allowed to form p-n junctions as well as heterogeneous structures by combining ZnTe with other n-type semiconductors [19, 21]. To date, some ZnTe nanostructures have been synthesized and the electrical properties were also investigated. Zhang et al. reported the synthesis of p-type single-crystal ZnTe nanoblets (NBs) in organic solutions [17]. That the ZnTe NWs core showed p-type electrical properties while the SiO<sub>x</sub> shell acted as an effective insulating layer was reported by Cao [22]. Li et al. reported the synthesis and the optical absorption band edge of ZnTe NWs arrays [23]. The dependence of the growth morphologies ZnTe nanostructure on temperature has been discussed by Meng et al. [24]. The p-type conductivity of ZnTe nanoribbons by nitrogen doping has been studied in our previous paper [25]. However, the electrical conductivity of twin ZnTe NW is not discussed up to present, particularly in the case of advanced nanoscaled device structures based on p-type twin NW.

In this paper, the synthesis of the periodic twin NW was explored, the twin ZnTe NWs were characterized by using field emission scanning electron microscopy, transmission electron microscopy, and a selected-area electron diffraction. The growth mechanism of the twin NW via the vapor–liquid–solid (VLS) growth was discussed. Then the p-type electrical conductivity and transfer properties based on nanofield-effect transistors (nano-FETs) were investigated. Significantly, the negative differential resistance was observed in twin ZnTe nano-FET, which can be explained by using the resonant tunneling among the periodic twin barriers. This study can develop the application of twin ZnTe NWs in new kind of nanoelectric devices.

## 2 Experimental

The twin ZnTe NWs were synthesized in an alumina tube furnace via thermal evaporation process. High-purity ZnTe powder (99.999%) was loaded into an alumina boat and then placed at the center of the quartz tube furnace. Si substrates coated with 20 nm gold catalyst were placed in the downstream direction from the ZnTe source. After the tube evacuated to a base pressure of 10<sup>-2</sup> Torr, the mixture of Ar and H<sub>2</sub> with a volume ratio of 90:10 was used as the carrier gas and kept at a constant flow rate of 60 standard cubic centimeters per minute (sccm), while the ZnTe source and the substrates were heated at a rate of 10 K min<sup>-1</sup> to 1100 K and 860 K, respectively. During the experiments, the pressure inside the tube was maintained at 600 Torr, the duration was 1 h.

Morphology and structure characterizations of the as-synthesized twin NWs were characterized by using field-emission scanning electron microscopy (FESEM, SIRION 200, FEI), X-ray diffraction (XRD, D/max-γB), transmission electron microscopy (TEM) and high-resolution transmission electron microscopy (HRTEM, JEM-2010, JEOL) with selected-area electron diffraction (SAED). The compositions of the nanowires were analyzed by energy-dispersive X-ray spectroscopy (EDX, OXFORD, equipped on the SEM).

To study the electrical properties of 1D periodic twin ZnTe NWs, the FETs based on the twin NW were constructed. For the preparation of FETs, ZnTe NWs were deposited on a degenerately doped silicon wafer with 300 nm dielectric of silicon dioxide. A mesh-grid consisted of 5 μm tungsten wire was used as the shadow mask and nickel electrodes (120 nm) were deposited in a high-vacuum electron-beam evaporation system. The electrical measurements were conducted by using a semiconductor characterization system (Keithley 4200) at room temperature.

## 3 Results and discussion

### 3.1 The synthesis and characterization of twin ZnTe nanowires

Figure 1a shows the SEM image of the as-synthesized periodic twin ZnTe NWs. Typically, the NWs have a uniform wire-like geometry, tens of micrometers in length, and 60–100 nm in diameter. From the high-magnification image in the top inset, the surface microtopography of the as-synthesized NWs is characterized as twin crystal. The bottom inset shows an EDX spectrum of the twin NWs, which reveals the presence of Zn, Te and Si (the Si peak comes from the Si substrate), the Zn:Te atomic ratio is semiquantitatively calculated to be about 43:57 revealing a large non-stoichiometry with many Zn vacancies, this result is the same as our early report [25]. Figure 1b is a typical low-magnification TEM image of the periodic twin ZnTe NW, which has a diameter of about 80 nm with clean and smooth surface. The measured angle between the two symmetrical planes is 141°, which repeats in every conjoint twin throughout the entire nanowire. Figure 1c shows the HRTEM image of twin nanowires, and Fig. 1d gives the corresponding SAED pattern recorded along the [011] zone axis, which consists of two sets of diffraction spots as indexed. The detailed electron diffraction analysis reveals that the NW has a twin relationship and shares a common (11-1) plane. The growth of NW is along [11-1] direction, and the angle between the (-1-1-1) facets of nanowires sidewall is 141°, the value of calculation is in well agreement with the measurement. In the XRD pattern as shown in Fig. 1e, all of

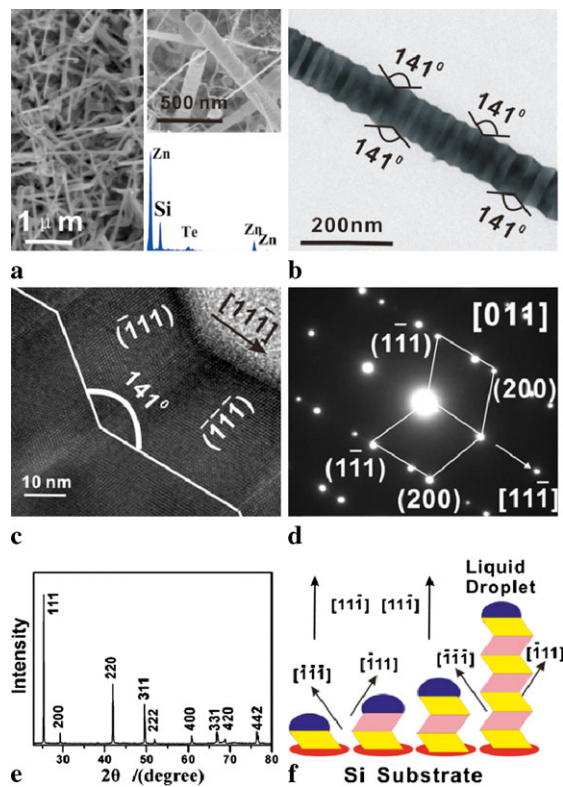


**Fig. 1** (a) The SEM image of the typical as-synthesized twin ZnTe NWs. The *top inset* is the high-magnification image; the *bottom inset* is an EDX spectrum of the twin NWs. (b) A typical low-magnification TEM image of the twin ZnTe NW. (c) The HRTEM image of twin ZnTe nanowire. (d) The corresponding SAED pattern recorded along the [011] zone axis. (e) XRD patterns of twin ZnTe nanowires. (f) The schematic diagram of the growth process of twin ZnTe NW

the detected peaks can be indexed to a standard diffraction card (JCPDS No. 15-0746), which indicates the twin of zinc blende structure (space group F-43m (216)).

The schematic diagram shown in Fig. 1f reveals the vertical cross-section of the growth process of ZnTe twin NW. The growth mechanism of ZnTe twin NW can be understood in view of the fundamental theory of thermodynamics and dynamics, respectively. The crystal preferentially grows via close-packed planes {111} to minimize the surface energy. Moreover, the formation of periodical twin can be attributed to the periodical surface tension coming from the eutectic liquid droplet. Usually the growth of NW is dominated by a gold catalyst VLS growth mechanism in thermal evaporation process. Without a doubt, the {111} planes of zinc-blende structure ZnTe have the lowest interface energy with the gold liquid droplet on the silicon substrate [13, 17, 24]. At elevated temperature, the source powder sublimates, and the resulting gas clusters or molecules of ZnTe and H<sub>2</sub> would hit reciprocally, then form active free-matrix, atomic-cluster, and molecular-cluster denoted as active particles [25]. When transported to the low-temperature regions by carrier gas and thermal diffusion, these active particles

will be adsorbed and diffuse to the surface of the gold-coated Si substrate, then land at a suitable site. Therefore, ZnTe will form eutectic cell structure with the gold liquid droplet [26]. As the absorbing process continues, the concentration of ZnTe in the droplet will become higher and exceed a critical level, then, the solid ZnTe precipitate at the interface between the liquid eutectic droplet and Si substrate. Due to the variable wet ability and surface tension of the catalyst liquid droplet and the solid ZnTe, most of the precipitated ZnTe crystals would form a {111} plane to minimize the surface energy, and align its {111} facets upward in the initial stage [13, 15, 24]. As more ZnTe vapor is absorbed into the metal liquid droplet, ZnTe continuously precipitate at the interface of the liquid droplet/ZnTe solid disk/rod to achieve a dynamic balance. The continuous precipitation will propel the axial growth of the NW and impel the liquid metal tip away from the substrate along the direction of  $\langle 111 \rangle$  to maintain the minimum surface energy of the crystal. On the other hand, the zinc blende ZnTe is a polar crystal with the atomic layer of Zn for a positive plane of (111) and the atomic layer of Te for a negative one of (-1-1-1). Because Zn has a higher saturated vapor pressure than Te, the composition of intrinsic ZnTe single crystal tends to the deviation toward the Te excess side [19, 25, 27], and the growth speed of these two planes is different, and the growing speed of atomic layer of Te is faster than that of the Zn layer. Thus, this alternative growth of different atomic layers can lead to the increase of periodical disturbance from the initial growth. It can be suggested that the initial close-packed plane is (11-1) shown in Fig. 1f, but under the integrated effect of various disturbance caused by the different growth speed of plane and the directional flow of carrier and thermal diffusion, the atoms of ZnTe precipitate along another close-packed plane of (-1-1-1) to reduce the surface energy. So, the expanding edges of plane of (-1-1-1) would push onto the left sidewall of the liquid droplet, and the layers of closed-packed plane (-1-1-1) are formed sequentially. Consequently, the plane formed progressively will lead to a high compressive stress with the increasing surface tension and restrain the further growth. Therefore, as the growth continues, the compressive stress will reach the critical level eventually. As a result, the close-packed growth along [-1-1-1] direction is stopped by surface tension of the liquid droplet, so it needs to choose another preferred growth direction. Interestingly, the closed-packed direction are changed from [-1-1-1] to [-111] to the right as shown in Fig. 1f. In this case, the compressive stress to the left will be released gradually. After layers of a close-packed plane formed progressively, the compressive stress to the right will reach the critical level, so the closed-packed direction will change once again from [-111] to [-1-1-1] to the left. Significantly, two close-packed planes of (-1-1-1) and (-111) are symmetric with a twin plane (11-1), and the angle between two symmetric planes is 141°; this angle agrees well with that shown in the TEM image Fig. 1b.

In short, the alternating stacking direction of atoms of ZnTe NW affected by repeating the alternative compressive stress leads to the formation of periodic twin NW and the thermodynamic balance of integral system. Furthermore, the integrated growth direction of twin is along symmetry center axis, i.e. [11-1].

### 3.2 Electrical properties

Electrical properties of 1D nanostructure sensitively depend on their structures, morphologies, and sizes. As one of the periodic superlattices structure, the twin ZnTe nanowires can present novel electronic transport characteristics. The nano-FETs are constructed based on a single ZnTe twin NW, and the electrical measurements are performed. The inset in Fig. 2a illustrates the device structure of the FET with the heavily doped p<sup>+</sup>-Si substrate and the SiO<sub>2</sub> layer (300 nm) serving as the back-gate and the gate dielectric, respectively. As shown in Fig. 2a, the typical source-drain current versus voltage ( $I_{ds}$ - $V_{ds}$ ) curves are obtained at varied gate voltages ( $V_g$ ) from -30 V to 10 V in a step of 10 V. It can be observed that the conductance of the NW monotonously increases with the decreasing of the  $V_g$ , such gate-dependent  $I_{ds}$ - $V_{ds}$  characteristics reveal the p-type conductivity of twin ZnTe NWs [25, 28]. Figure 2b shows the corresponding transfer characteristics ( $I_{ds}$ - $V_g$ ), which depicts

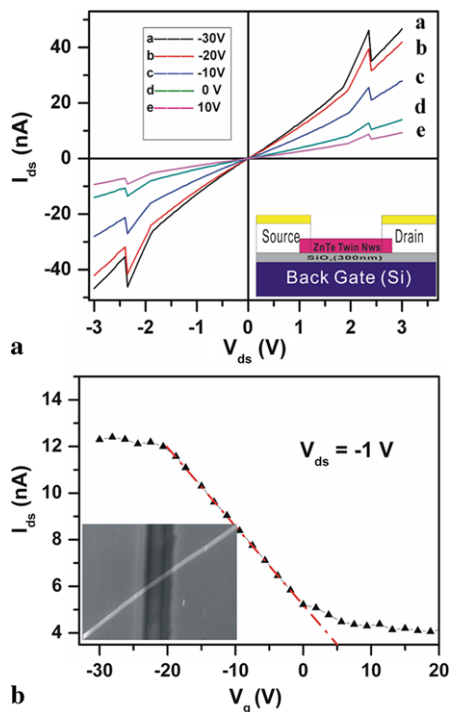


**Fig. 2** Electron transfer characteristics of twin ZnTe NW FET. (a)  $I_{ds}$  vs.  $V_{ds}$  curves for different  $V_g$  that range from 10 to -30 V. The inset is a schematic diagram of twin ZnTe NWs FET. (b)  $I_{ds}$  vs.  $V_g$  curve measured at  $V_{ds} = -1$  V. The inset is the SEM image of a typical twin NW FET device

the  $I_{ds}$ - $V_g$  curve at  $V_{ds} = -1$  V. The SEM image for a typical device is shown in the inset of Fig. 2b. The hole mobility ( $\mu_h$ ) can be deduced from the equation,  $g_m = \mu_h L^2 / CV_{ds}$  [29]; here,  $g_m$  ( $g_m = dI_{ds}/dV_g$ ) is the transconductance in the linear region ( $V_g$  from -20 V to 0 V), and the value is about 0.34 nS,  $C$  is the capacitance of the NW, and  $L$  the length of the NW channel of 4800 nm. The capacitance can be given by  $C = 2\pi\epsilon_0\epsilon_{SiO_2}L/\ln(4h/d)$ , here  $\epsilon_{SiO_2}$  is the dielectric constant (3.9 for SiO<sub>2</sub>);  $h$  is its thickness, and  $d$  the NW diameter of 80 nm. Taking account of the diameter ( $d$ ) and gate length ( $L$ ), the capacitance ( $C$ ) can be calculated to be 0.72 fF. To put these values into the above equation,  $\mu_h$  can be deduced to be about 0.11 cm<sup>2</sup> V<sup>-1</sup> S<sup>-1</sup>. This value is close to that of single crystalline ZnTe NWs reported in the literature [30], but much lower than the value of ZnTe thin film [31]. The resistance of ZnTe twin NW ( $R$ ) is estimated to be about  $5 \times 10^9 \Omega$  and resistivity ( $\rho$ ) is about 520  $\Omega$  cm by taking account of the dimensions of the twin NW. The hole concentration ( $n_h$ ) thus can be estimated to be about  $1.1 \times 10^{17}$  cm<sup>-3</sup> from the relations of  $\rho = 1/n_h e \mu_h$ . By extrapolating the  $I_{ds}$ - $V_g$  curve to  $V_g$  axis, the threshold voltage ( $V_{th}$ ) is estimated to be 5 V. In fact, the p-type behavior of the intrinsic ZnTe NWs is attributed to the intrinsic defects such as Zn vacancies in the twin NWs due to the self-compensation effect [19, 21, 25], but the carrier concentration and mobility are different from our report [25] due to the different crystal structure and morphology. The defect theory can be used to explain the p-type conductivity of the twin ZnTe NWs [23, 25], and then the neutral Zn vacancy of  $V_{Zn}^x$  and the ionized vacancies will bring about the acceptor energy level in the forbidden energy gap. Meanwhile, the holes can be generated at the top of valence band, which contribute to the p-type conductivity.

It is worth noting that a series of negative differential resistance (NDR) are observed at source-drain voltages ( $V_{ds}$ ) range from -1.9 V to -2.4 V and 1.9 V to 2.4 V, respectively, which monotonously increase with the decreasing of the gate voltages ( $V_g$ ) from 10 V to -30 V. As shown in Fig. 2a, the peak-value voltage ( $V_p$ ) is at 2.3 V, and the valley-value voltage ( $V_v$ ) is at 2.4 V. Accordingly, both the peak-value current ( $I_p$ ) and the valley-value current ( $I_v$ ) increase with the decreasing of the gate voltage ( $V_g$ ). The peak-to-valley current ratios are estimated to be about 1.3, which is close to that of carbon nanotube [32].

The theory of tunneling in 1D has been presented in almost all quantum mechanics textbook. The first tunneling diode or Esaki diode was discovered by Esaki in 1958 [33]. Esaki and Tsu suggested that a superlattice can also form NDR in 1973 [34], and NDR in a GaAs/AlAs superlattice was achieved in 1990 [35]. Up to now, the NDR has been demonstrated in nanoelectronic device, the resonant tunneling quantum-well at frequencies as high as 2.5 THz of GaAs has been observed by Sollner et al. [36]. In addition, negative differential resistances in carbon nanotube field-effect

transistors (FET) have been demonstrated [32, 37]. But all the NDR reported above are achieved in the heterogeneous structure and diodes, which can be explained by coherent tunneling and sequential tunneling theory. In our experiments, the NDR is first observed in twin ZnTe NW, but this occurrence is different with that of heterogeneous structure. The interface between the different close-packed planes behave like the energy potential barriers and impede the electron transmission, the periodic potential well between two barriers can be formed in series along 1D NW direction. From the HRTEM image shown in Fig. 1c, the length between two barrier planes is only about 18 nm, which is shorter than the value of  $\mu\tau$  ( $\mu$  is the mobility,  $\tau$  the transmit time), so the continuous energy band can be split and form discrete energy level due to the quantum effect. Under the effect of external electrical field, the energy level can slope to a certain extent. The resonant tunneling can occur when the energy of some electrons reaches one sloped energy level, and the current becomes large, and the NRD appears.

The current of twin NW can be divided into two parts: the intrinsic current ( $I_{in}$ ) and the resonant tunneling current ( $I_{RT}$ ). The  $I_{in}$  mainly includes the thermoelectron emission current ( $I_{th}$ ) and the inelastic tunneling current ( $I_{IT}$ ). Both  $I_{IT}$  and  $I_{th}$  increase monotonically with the increasing bias. In particular, the  $I_{th}$  is intensively dependent on the temperature, and becomes the main component at high bias. However, if it meets the resonant tunneling condition, the  $I_{RT}$  will play a remarkable role in the electrical conductivity. These characteristics imply that the enhancement of space charge is available for modulating the interfaces barrier with the inherent feedback mechanism of resonant tunneling in 1D multi-barrier nanostructure. To illustrate the tunneling process simply, a model for resonant tunneling can be applied to the NDR of p-type ZnTe twin NWs as shown in Fig. 3a. This is a schematic diagram of one three-barrier coherent-tunneling model, the potential barriers on the twin grain boundary behave like the semi-transmitted reflective mirror, and the quantum well between two potential barriers correspond to one mirror reflection resonant cavity which can be thought as Fabry–Perot resonant cavity [38]. The tunneling process of electrons includes entering into resonant cavity, multireflection between two reflective mirrors, and transmitting across the barrier. Here, the tunneling current is in phase with the field due to the similar wells and barriers. The conception of electronic wave can be used to demonstrate the physical processes of the resonant tunneling, Fig. 3b is considered as an illustration under the effect of electric field. The electron with energy of  $E_1$  in region A through potential barrier  $B_1$  inject into potential well  $W_1$ , and then the electronic waves arrive in the potential barrier  $B_2$  along the 1D direction. Partial electronic waves transmit  $B_2$ ,  $W_2$ , and  $B_3$  and so on. Meanwhile, part of them reflects to  $W_2$  along reverse direction, a part transmits  $B_2$  and  $W_1$

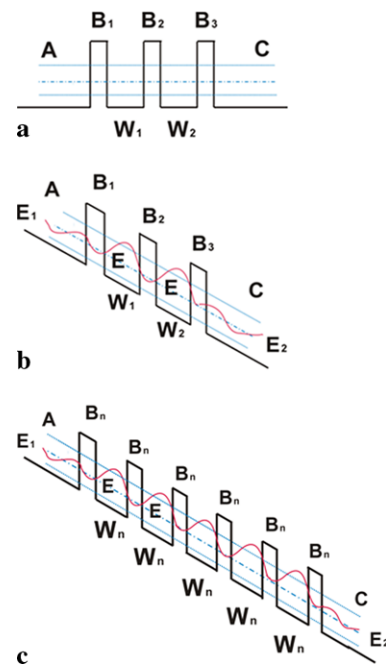


**Fig. 3** The schematic diagram of resonant tunneling effect. **(a)** A three-barrier coherent-tunneling model of resonant tunneling. **(b)** An illustration of the three-barrier coherent-tunneling model under the effect of electric field. **(c)** The multibarrier model of resonant tunneling

back to region A, and a part reflects back to  $W_1$ . In effect, the electrons on the potential well energy level will resonate with a velocity of  $V = \frac{\hbar k}{2\pi m^*}$  between two barriers,  $B_1$  and  $B_2$  or  $B_2$  and  $B_3$ , etc. If it meets the resonant condition of  $E = E_0$  ( $E_0$  the corresponding resonant energy), the amplitudes of electronic waves will be enhanced and reach the maximum gradually after multi-reflection. Meanwhile, with the amount of electron trapped into the well increasing, the oscillating currents will reach to the stationary states as well as self-accelerating under the condition of resonant tunneling. Furthermore, the integrated transmission coefficient  $T$  depends on transmittance  $T_x$  of every potential barrier [39], the relation can be express as  $T = \frac{4T_1T_2}{(T_1+T_2)^2}$ , where  $T_1$  is the transmittance of first barrier, and  $T_2$  of the second. When the energy  $E = E_0$ ,  $T_1 = T_2$ , and so  $T = 1$ , the resonant current will reach the maximum. However, if  $E \neq E_0$ , the electronic waves cannot meet the resonant condition. Indeed, the integrated transmittance  $T = T_1T_2$ , and then both the value of  $T_1$  and  $T_2$  are exponential small numbers, so the value of  $T_1T_2 \ll 1$ . Similarly, the three-barrier module can be extended to the multibarrier model as shown in Fig. 3c.

The resonant tunneling is not only dependent on the barrier height and width, but on the energy distributions of potential well. In the quantum mechanics point of view, the conduction band (or valence band) is split into discrete subbands in a quantum well being proportional to the well width of  $L^2$ . The rectangular potential-energy barriers within the

well (such as shown in Fig. 3a) along with 1D direction is given by  $E_{n_x} = \frac{h^2 n_x^2}{8m^* L_x^2}$  ( $n_x = 1, 2, 3, \dots$ ), where  $h$  is Plank constant,  $m^*$  effective mass of electron,  $L_x$  width of the well. In the case of no bias, the electron energy  $E$  is above  $E_1$  (the high energy side under electrical field condition), so that resonant tunneling cannot occur. When the bias voltage is added, energy band slopes downward. Thus, the  $E$  decreases to the value below the  $E_1$ , resonant tunneling starts and this voltage is denoted threshold voltage ( $V_T$ ). As the bias increase, the  $E$  is pulled to the special energy band the  $E_0$  (below the  $E_1$  and above the  $E_2$  (the low energy side under electrical field condition)). Then the resonant tunneling would be induced by the two equivalent energy bands the  $E$  and the  $E_0$ . The resonant current will be enhanced with the increase of the bias. When the bias reaches to the peak value ( $V_p$ ), resonant current arrives at the peak value ( $I_p$ ). If the bias increases continually, the resonant tunneling effect decreases gradually and the resonant current declines to zero. Meanwhile, the  $E$  decreases into the low energy level below the  $E_2$ . In summary, it is reasonable to conclude that the periodic barriers produced in the periodic twin interfaces form multi-well along 1D direction. Under the influence of an electric field, if it meets the resonant condition, the space charge could be enhanced in Fabry–Perot resonant cavity by modulating the interfaces barrier with the inherent feedback mechanism, accordingly, the NRE contributes to the significant change of the current in the twin p-type ZnTe NWs FET.

#### 4 Conclusion

The resonant tunneling in twin p-type ZnTe NW FET has been studied. The periodic twin ZnTe NWs were synthesized via a conventional thermal evaporation process. The characterization reveals that the twin ZnTe NW has the zinc-blende crystal structure with the common growth direction of [11-1], and more than ten micrometers in lengths. The formation mechanism of periodic twin can be attributed to the alternative surface tension of the eutectic liquid droplet. The electrical measurements of nano-FET based on single twin NW indicate that the twin NW has the p-type semiconducting characteristic with the carrier concentration ( $n_h$ ) of  $1.1 \times 10^{17} \text{ cm}^{-3}$ , mobility of  $0.11 \text{ cm}^2 \text{ V}^{-1} \text{ S}^{-1}$  and the threshold voltage of 5 V. It is significant that the negative differential resistance induced the resonant tunneling is observed in single p-type twin ZnTe NW FET. The semi-quantitatively measurement demonstrates that the peak-value voltage ( $V_p$ ) is at 2.3 V, the valley-value voltage ( $V_v$ ) at 2.4 V, and the peak-to-valley current ratio is about 1.3. The resonant tunneling can be attributed to the periodic barrier produced in the periodic twin interface. Under the

influence of an electric field, the space charge could be enhanced by modulating the interfaces barrier with the inherent feedback mechanism in 1D multi-barrier nanostructure. These results above can offer a new resonant tunneling prototype based on the single p-type twin ZnTe NWs, and will promote the application of twin ZnTe NW in nanoelectric device.

**Acknowledgements** We thank the financial support from the Nation High Technology Research and Development Program of China (No. 2007AA03Z301), the Natural Science Foundation of China (No. 20771032 and No. 61076040) and Anhui Province (070414200), Henan Province (092102210198), and the National Basic Research Program of China (No. 2007CB936001).

#### References

1. R. Agarwal, C.M. Lieber, *Appl. Phys. A, Mater. Sci. Process.* **85**(3), 209 (2006)
2. C.M. Lieber, Z.L. Wang, *Mater. Res. Soc. Bull.* **32**(2), 99 (2007)
3. D. Zhang, S. Chava, C. Berven, S.K. Lee, R. Devitt, V. Katkanant, *Appl. Phys. A, Mater. Sci. Process.* **100**(1), 145 (2010)
4. Z.L. Wang, J.H. Song, *Science* **312**(5771), 242 (2006)
5. J. Yu, H.Q. Yang, R.Y. Shi, L.H. Zhang, H. Zhao, X.W. Wang, *Appl. Phys. A, Mater. Sci. Process.* **100**(2), 493 (2010)
6. X.Y. Chen, C.T. Yip, M.K. Fung, A.B. Djuricic, W.K. Chan, *Appl. Phys. A, Mater. Sci. Process.* **100**(1), 15 (2010)
7. B.Z. Tian, X.L. Zheng, T.J. Kempa, Y. Fang, N.F. Yu, G.H. Yu, J.L. Huang, C.M. Lieber, *Nature* **449**, 885 (2007)
8. I. Enculescu, M.E. Toimil-Molares, C. Zet, M. Daub, L. Westerber, R. Neumann, R. Spohr, *Appl. Phys. A, Mater. Sci. Process.* **86**(1), 43 (2007)
9. S.H. Lee, X.-G. Zhang, B. Smith, S.S.A. Seo, Z.W. Bell, J. Xu, *Appl. Phys. Lett.* **96**(19), 193116 (2010)
10. Y. Hao, G. Meng, Z.L. Wang, C. Ye, L. Zhang, *Nano Lett.* **6**(8), 1650 (2006)
11. B.Y. Geng, X.W. Liu, Q.B. Du, X.W. Wei, L.D. Zhang, *Appl. Phys. Lett.* **88**(16), 163104 (2006)
12. B. Liu, Y. Bando, M. Liao, C. Tang, M. Mitome, D. Golberg, *Cryst. Growth Des.* **9**(6), 2790 (2009)
13. X. Fan, X.M. Meng, X.H. Zhang, M.L. Zhang, J.S. Jie, W.J. Zhang, C.S. Lee, S.T. Lee, *J. Phys. Chem. C* **113**(3), 834 (2008)
14. F.M. Davidson, D.C. Lee, D.D. Fanfair, B.A. Korgel, *J. Phys. Chem. C* **111**(7), 2929 (2007)
15. Y.Q. Wang, U. Philipose, T. Xu, H.E. Ruda, K.L. Kavanagh, *Semicond. Sci. Technol.* **22**(3), 175 (2007)
16. Y. Ding, Z.L. Wang, *Micron* **40**(3), 335 (2009)
17. J. Zhang, P.C. Chen, G.Z. Shen, J.B. He, A. Kumbhar, C.W. Zhou, J.Y. Fang, *Angew. Chem., Int. Ed. Engl.* **47**(49), 9469 (2008)
18. Q.F. Meng, C.B. Jiang, S.X. Mao, *Appl. Phys. Lett.* **94**(4), 043111 (2009)
19. T.A.K. Sato, M. Hanafusa, A. Noda, A. Arakawa, M. Uchida, O. Oda, Y. Yamada, T. Taguchi, *Phys. Status Solidi A* **180**(1), 267 (2000)
20. N. Tit, *J. Vac. Sci. Technol.* **22**(3), 821 (2004)
21. V.S. John, T. Mahalingam, J.P. Chu, *Solid-State Electron.* **49**(1), 3 (2005)
22. Y.L. Cao, Y.B. Tang, Y. Liu, Z.T. Liu, L.B. Luo, Z.B. He, J.S. Jie, R. Vellaisamy, W.J. Zhang, C.S. Lee, S.T. Lee, *Nanotechnology* **20**(45), 455702 (2009)
23. L. Li, Y.W. Yang, X.H. Huang, G.H. Li, L.D. Zhang, *J. Phys. Chem. B* **109**(25), 12394 (2005)

24. Q.F. Meng, C.B. Jiang, S.X. Mao, *J. Cryst. Growth* **310**(20), 4481 (2008)
25. S. Li, Y. Jiang, D. Wu, L. Wang, H. Zhong, B. Wu, X. Lan, Y. Yu, Z. Wang, J. Jie, *J. Phys. Chem. C* **114**(17), 7980 (2010)
26. E. Janik, P. Dluzewski, S. Kret, A. Presz, H. Kirmse, W. Neumann, W. Zaleszczyk, L.T. Baczewski, A. Petrouchik, E. Dynowska, J. Sadowski, W. Caliebe, G. Karczewski, T. Wojtowicz, *Nanotechnology* **18**(47), 475606 (2007)
27. D. Bensahel, M. Dupuy, J.C. Pfister, *J. Cryst. Growth* **47**(5–6), 727 (1979)
28. G.D. Yuan, Y.B. Zhou, C.S. Guo, W.J. Zhang, Y.B. Tang, Y.Q. Li, Z.H. Chen, Z.B. He, X.J. Zhang, P.F. Wang, I. Bello, R.Q. Zhang, C.S. Lee, S.T. Lee, *ACS Nano* **4**(6), 3482 (2010)
29. G.D. Yuan, W.J. Zhang, J.S. Jie, X. Fan, J.A. Zapien, Y.H. Leung, L.B. Luo, P.F. Wang, C.S. Lee, S.T. Lee, *Nano Lett.* **8**(8), 2591 (2008)
30. H.B. Huo, L. Dai, C. Liu, L.P. You, W.Q. Yang, R.M. Ma, G.Z. Ran, G.G. Qin, *Nanotechnology* **17**(24), 5912 (2006)
31. D. Bhattacharyya, S. Chaudhuri, A.K. Pal, *Mater. Chem. Phys.* **40**(1), 44 (1995)
32. M. Rinkiö, A. Johansson, V. Kotimäki, P.i. Törmä, *ACS Nano* **4**(6), 3356 (2010)
33. L. Esaki, *Phys. Rev.* **109**(2), 603 (1958)
34. R. Tsu, L. Esaki, *Appl. Phys. Lett.* **22**(11), 562 (1973)
35. A. Sibille, J.F. Palmier, H. Wang, F. Mollot, *Phys. Rev. Lett.* **64**(1), 52 (1990)
36. T.C.L.G. Sollner, W.D. Goodhue, P.E. Tannenwald, C.D. Parker, D.D. Peck, *Appl. Phys. Lett.* **43**(6), 588 (1983)
37. S.W. Lee, A. Kornblit, D. Lopez, S.V. Rotkin, A.A. Sirenko, H. Grebel, *Nano Lett.* **9**(4), 1369 (2009)
38. D.J. Gargas, M.C. Moore, A. Ni, S.-W. Chang, Z. Zhang, S.-L. Chuang, P. Yang, *ACS Nano* **4**(6), 3270 (2010)
39. B. Ricco, M.Y. Azbel, *Phys. Rev. B* **29**(4), 1970 (1984)